Inversion Procedure and Resolution Tests

For all of the inversions discussed in this paper, we employed the Modular system for EM inversion (ModEM; Egbert and Kelbert, 2012). ModEM is a modular Fortran 95 code suitable for general-purpose electromagnetic inversion. It features several inversion algorithms that can be used interchangeably, parallelization over transmitters and polarizations, and a novel and flexible model covariance scheme which penalizes deviations from a specified prior model. In this application, we fit both the full impedance tensor and the vertical magnetic transfer functions at all sites.

We run non-linear conjugate gradient inversion algorithm in parallel on 15 processors. Due to non-linearity of the problem, this algorithm requires iteration to converge. Each of the inversion runs we performed took approximately 120–140 iterations to fit the data to a normalized RMS < 2 with 5% error floors on the impedances and 0.05 error floors on the vertical magnetic field transfer functions. For final inversions, we tightened the error floors on the vertical field transfer function components to 0.03. We have allowed the inversion to insert small-scale anomalies in the upper 4-5 km to account for near-surface structure, but do not attempt to interpret results at shallow depths, given the wide site spacing.

Our preferred solution, generated using a uniform 200 Ωm half space as the prior model for the inversion, fit the data to a normalized root mean square misfit (RMS) of 1.89 (1.97 for the full data set, before removal of the poor quality data points). This model is shown in Figures 2 and 3 in the main text. Since the 3D MT inversion is inherently non-unique, alternative inversions were also run to test our depth resolution and to thereby justify our interpretation.

Multiple inversions (10–15 total) were run with a range of *a priori* constraints, including varying degree of smoothing, different vertical and horizontal gridding and a range of other prior and initial models. Prior model assumptions were specifically varied to establish robustness of features appearing in the inverse solutions. These prior models were either a uniform half space or a layered 1D resistivity. Figs. S1 and S2 provide a view of Model 2, obtained with a smooth one-dimensional prior model, with electrical resistivity decreasing logarithmically with depth starting at 200 Ωm, to

100 Ωm at 8 km depth, to 20 Ωm at 200 km, to 8 Ωm at 900 km depth at the bottom of the computational domain. Overall, this prior model was significantly more conductive than the 200 Ωm half space used for the preferred Model 1. Model 2 fits the cleaned data set to an RMS of 2.03 (RMS for full data set is 2.08). Figs. S3 and S4 provide a view of Model 3, obtained with an *a priori* assumption that the crust (above 42 km depth) is less resistive (60 Ωm) than the mantle, which was 200 Ωm. The RMS for Model 3 is 1.94 (1.99 with the full data set). Finally, Fig. S5 provide three representative (in terms of the sounding curves) data fits for the preferred Model 1.

Three-dimensional MT checkerboard resolution tests of relevant spatial extent and data distribution (e.g., Egbert and Kelbert, 2012; Figure 5) show that in ideal conditions (no near-surface distortions), the locations and magnitudes of the large-scale conductive features within the study area would be well resolved. Edges of the deeper conductors would be smoothed by the model regularization. The resistive features, including those beneath a conductor, would still be resolved, but the magnitudes would be underestimated.

Synthetic forward modelling tests were also run to ascertain whether specific features (such as a strongly conductive deep plume similar to that in Zhdanov et al., 2011) would affect the data to a significant extent. These tests suggest that the MT data would be highly sensitive to a deep plume-like conductor.

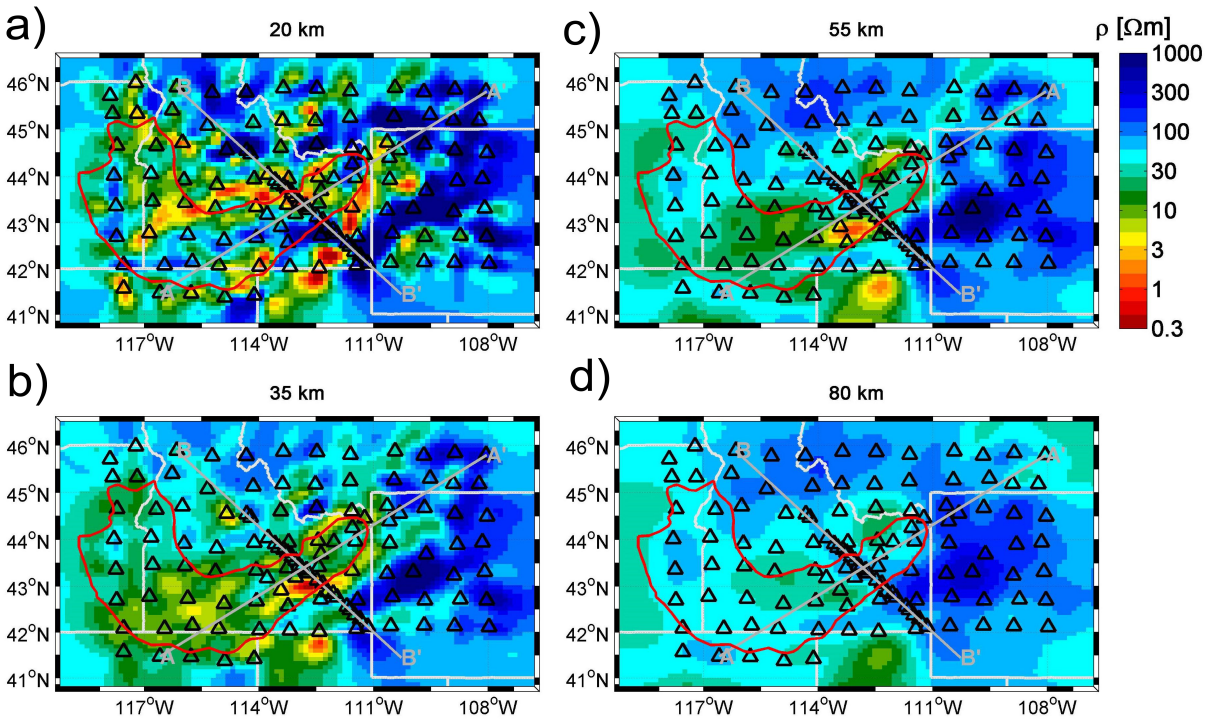

Figure 1: S1. Inverse model obtained by assuming higher *a priori* conductivities, at representative depths in the lower crust and uppermost mantle. The lines indicate the locations of the profiles AA' and BB' shown in Figure S2. The red contour outlines the Snake River Plain.

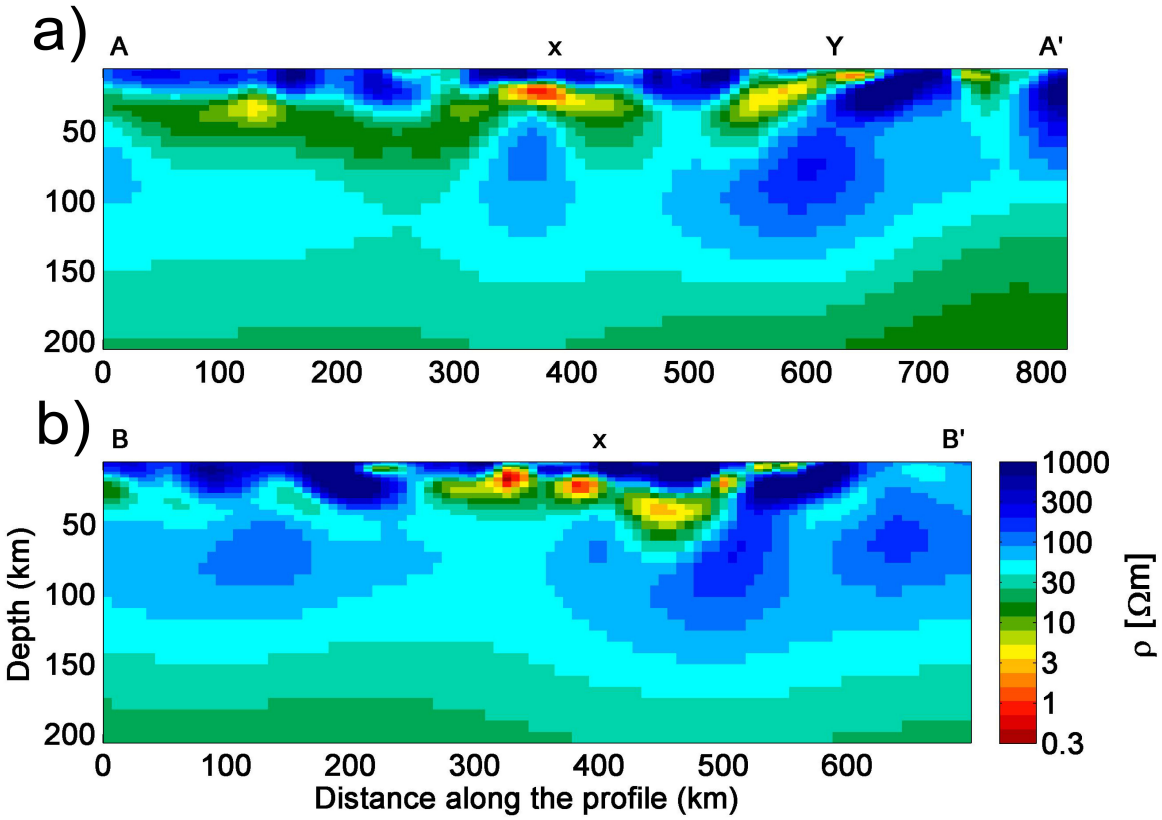

Figure 2: S2. Cross-sections from Figure S1 along (AA') and across (BB') the eastern Snake River Plain.

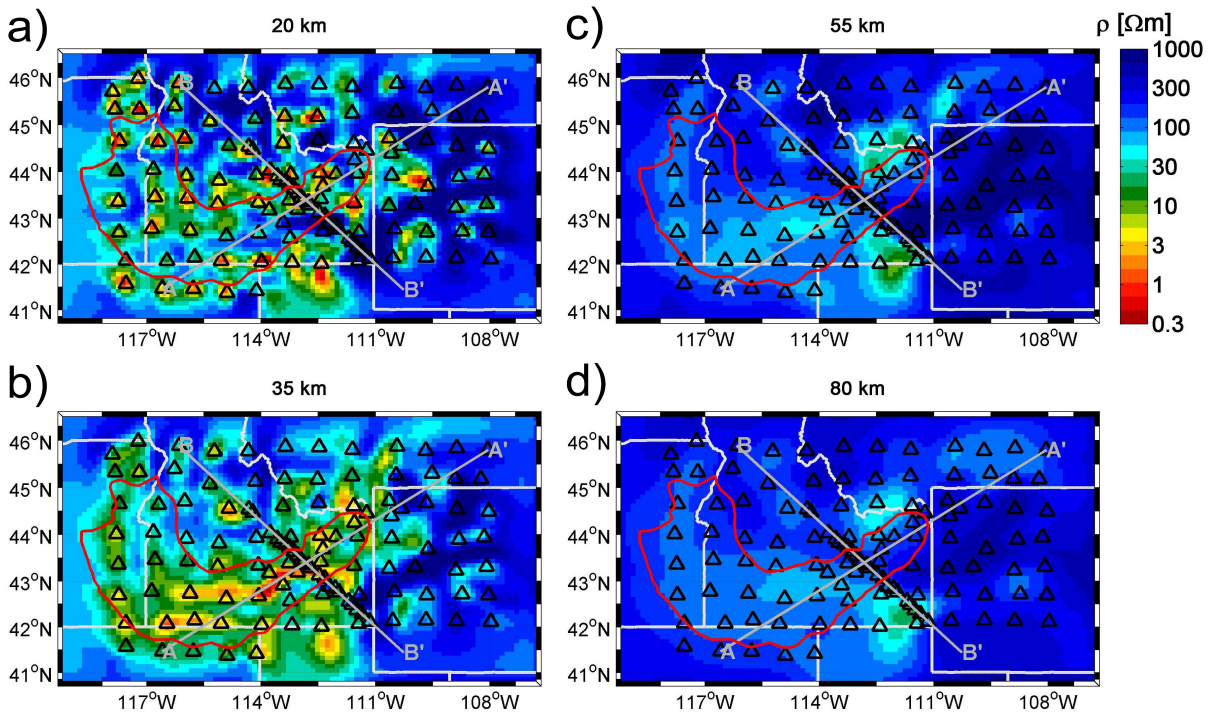

Figure 3: S3. Inverse model obtained by preferentially inserting high conductivities in the crust, at representative depths in the lower crust and uppermost mantle. The lines indicate the locations of the profiles AA' and BB' shown in Figure S4. The red contour outlines the Snake River Plain.

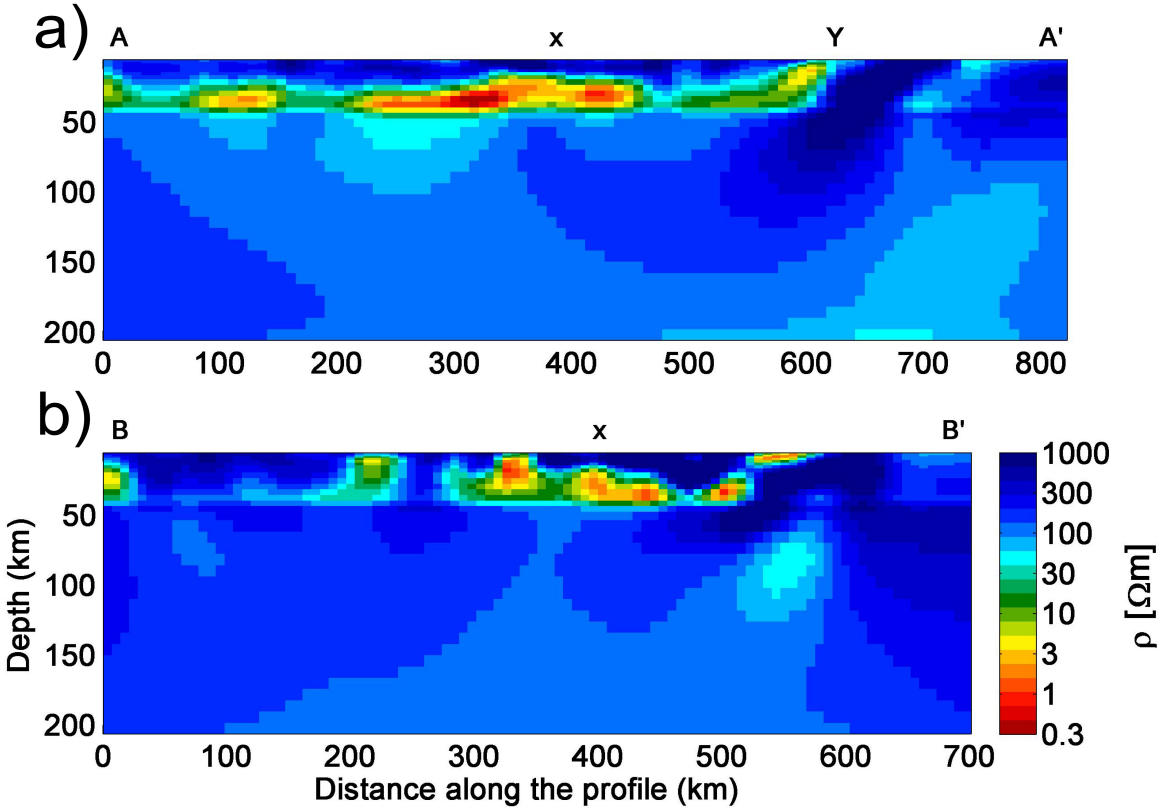

Figure 4: S4. Cross-sections from Figure S3 along (AA') and across (BB') the eastern Snake River Plain.

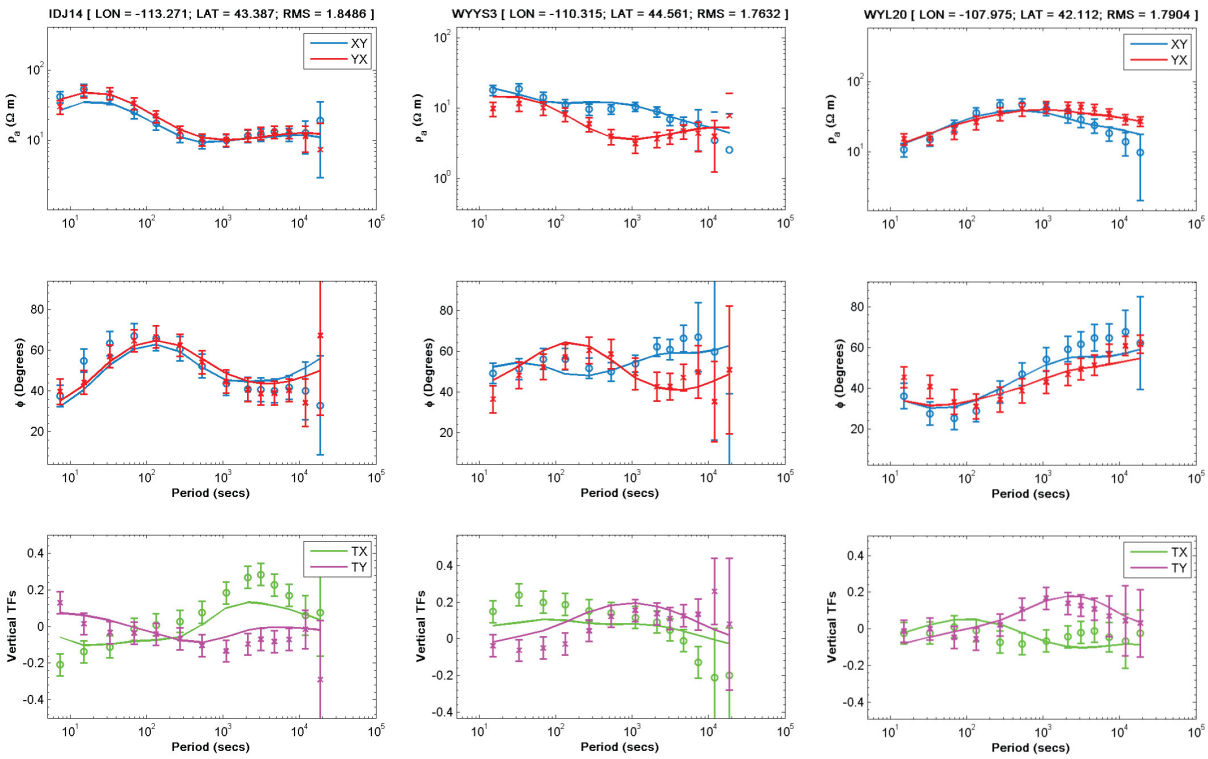

Figure 5: S5. Three representative apparent resistivity and vertical magnetic field transfer function curves with model fits and 5% error floors on the apparent resistivities and phases, and 0.03 error floors on the magnetic field transfer functions. The locations of the sites are central SRP (IDJ14), Yellowstone caldera (WYYS3) and the Wyoming craton (WYL20). Sounding curves in and around Yellowstone caldera differ significantly among themselves, indicating subsurface complexity.